POLITECNICO
MILANO 1863

DIPARTIMENTO DI MECCANICA

mecc

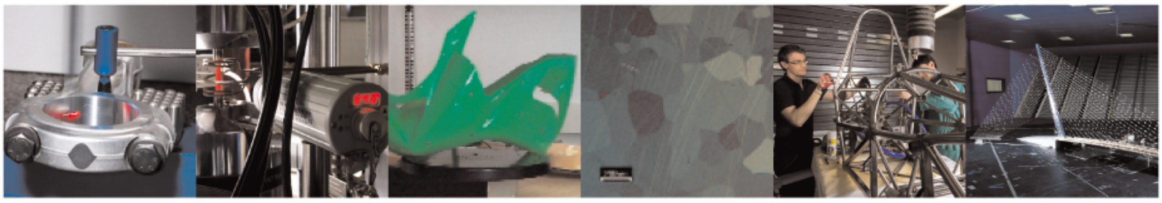

Analytical and empirical methods for the characterisation of the permanent transverse displacement of quadrangular metal plates subjected to blast load: Comparison of existing methods and development of a novel methodological approach

Lomazzi L.;Giglio M.;Manes A.

This is a post-peer-review, pre-copyedit version of an article published in International Journal of Impact Engineering. The final authenticated version is available online at: https://doi.org/10.1016/j.ijimpeng.2021.103890

DIPARTIMENTO DI MECCANICA ■ POLITECNICO DI MILANO
via G. La Masa, 1 ■ 20156 Milano ■ EMAIL (PEC): pecmecc@cert.polimi.it
http://www.mecc.polimi.it
Rev. 0

Analytical and empirical methods for the characterisation of the permanent transverse displacement of quadrangular metal plates subjected to blast load: comparison of existing methods and development of a novel methodological approach.

L. Lomazzi[1], M. Giglio[1], A. Manes[1]*

[1]Politecnico di Milano, Department of Mechanical Engineering, Via La Masa n.1, Milan, Italy

*Corresponding author: andrea.manes@polimi.it

E-mail addresses: luca.lomazzi@polimi.it (L. Lomazzi), marco.giglio@polimi.it (M. Giglio), andrea.manes@polimi.it (A. Manes).

Abstract

The behaviour of blast loaded structures has been extensively investigated over the past fifty years through experimental tests. These tests are quite challenging and require dedicated infrastructures to be efficiently and safely performed, however, the obtained data are useful to develop predictive approaches. Among them, analytical approaches are capable of efficient and satisfactory characterisation of blast events and the related effects on structures. In particular, among the analytical methods two categories can be identified: those methods exploiting fully analytical relationships, e.g., the Jones' theory, and those based on model fitting to experimental results, e.g., the Nurick and Martin's method. More recently, numerical models have been proposed to define the response of structures to blast loads: the main numerical methods considered to assess the structural response to blast loading are the coupled Eulerian-Lagrangian, uncoupled Eulerian-Lagrangian and Analytical-Lagrangian analyses. In this context, this paper aims at establishing a detailed comparison of the main fully analytical and empirical methods available in the literature, exploiting consolidated experimental evidence and results from numerical simulations. The focus of this work is on the estimation of the permanent transverse deflection of a quadrangular, initially flat plate subjected to blast loading, considering both close-range and far-field explosions. Moreover, a modelling framework is herein presented, which serves as a fast and reliable predictive tool for estimating blast load effects on plates.

Keywords: blast; structure; transverse displacement; models; impulsive loading.

1 Introduction

The behaviour of blast loaded structures has been largely studied in the last fifty years through experimental tests. These tests are quite challenging and require dedicated infrastructures to be efficiently and safely performed. Nevertheless, they have been exploited to establish new analytical characterisation methods of the blast wave propagation and its interaction with a target structure (e.g., [1] [2] [3] [4]), leading to the definition of some modelling approaches capable of satisfactorily characterise explosive events. These modelling approaches can be split into two categories, namely those characterising the phenomenon exploiting fully analytical methods and those involving empirical relationships obtained through model fitting to experimental results. More recently, numerical models and several finite element techniques have been proposed and verified to define the response of structures to blast loads. Some of these methods were compared by Børvik in the work in [5], they can be divided into three main categories: coupled Eulerian-Lagrangian, uncoupled Eulerian-Lagrangian and Analytical-Lagrangian analysis. The former class consists of characterising the blast wave through the Jones-Wilkins-Lee equation of state (JWL EOS) [6], exploiting Eulerian elements for the wave propagation, coupled with the evaluation of the response of the impacted Lagrangian structure, allowing to consider the mutual blast wave-structure interaction. Uncoupled Eulerian-Lagrangian analyses are less resource-demanding than coupled analyses since they do not consider the influence of the structural response on the blast wave properties. Finally, the latter class of approaches characterises the blast wave and its interaction with the impacted target analytically. The structural response is then determined exerting on the structure the pressure-time history that arises from some analytical interface models (e.g., [7]). However, the computational effort required by such numerical analyses is far more expensive than that typical of fully analytical methods. In fact, in case of complex geometries or large-scale explosions, the former requires up to days of computations, while the latter provide instantaneous results. Hence, even though numerical models are potentially more accurate, analytical and empirical approaches may provide results in less time with a satisfactory level of accuracy, especially if simple structures are considered. In the following, a literature review of analytical and empirical methods useful to address quadrangular plates subjected to blast loading is reported. No explicit reference is made to circular plates since they are not considered in this work.

Among the published fully analytical methods, it is worth citing the one based on the work by Jones [8]. In this work, a general approximate theoretical procedure for characterising the dynamic behaviour of arbitrarily shaped ductile metal plates subjected to a rectangular shaped pressure-time history was reported. The procedure considered the effects of finite deflections on the dynamic plastic behaviour of plates, retaining in the analysis both membrane forces and geometry change effects, while assuming a rigid, perfectly plastic material constitutive law. The theoretical work involved time-independent displacement profiles similar in shape to the respective static collapse fields. The theoretical predictions were compared to the experimental results reported in [9] and

[10], showing general good agreement with the measured transverse displacement in case no tearing occurred. The theory was further improved in 1992 by Yu and Chen [11] exploiting a more accurate description of the effects arising in the transient phase. This improvement was achieved by introducing a kinematically admissible time-dependent velocity field to trace the transient phase of the plate motion under dynamic loading. This refined analytical theory led to more accurate permanent deflection predictions in case of transverse displacements of the same order of magnitude of, or even greater than, the plate thickness. However, since this refined theory still neglected (i) the material strain rate sensitivity, (ii) strain-hardening effects, (iii) the influence of membrane stretching on the geometry and (iv) the shear force effect on the yield criterion, it provided satisfactory predictions only for deflections δ up to 5-10 times the plate thickness t. However, strain rate sensitivity is quite relevant to the maximum permanent transverse displacement of a plate, as shown in early works in this field (e.g., [12]). For instance, Perrone and Bhadra in 1979 developed a method to determine the response of a beam, modelled as an impulsively loaded string supported mass, while accounting for the material strain rate sensitivity [13]. Similarly, more recently Jones refined the theory presented in the work in [8] including material strain rate effects to improve the prediction accuracy of the transverse permanent displacement of dynamically loaded plates [14]. Later on, Jones compared the theoretical predictions from the aforementioned refined theory to some experimental results [15]. Moreover, in the same work, the Perrone and Bhadra's strain rate theory was extended to plates. This work showed that accounting for strain rate effects leads to the improvement of the overall accuracy of the permanent transverse deflection prediction of impulsively loaded plates. To the authors' best knowledge, no more advanced thorough theory has been developed yet in this analytical framework.

Within the class of empirical methods, dimensionless numbers have been extensively used to compare experimental results involving targets of different dimensions. One of the early proposed numbers was the dimensionless damage number α defined by Johnson [16]. This represented a general tool to assess the behaviour of metals under impact scenarios. However, it only considered the impact velocity of the threat, along with the target material density and damage stress. Hence, the number was modified by Nurick and Martin in the two-part work in [17] [18], expressing the impact velocity as a function of the impulse imparted to the plate, including the target geometrical characteristics and the plate loading area to total area ratio, the latter considered in case of circular geometry only. These improvements led to a new dimensionless number ϕ considering the blast, the plate material and the plate geometric characteristics. The number was developed to describe the deflection-thickness ratio of materials different in nature, i.e., steel and aluminium, employing a simple and unique empirical equation. The equation was presented in the same work for circular plates and quadrangular plates fully clamped at the edges, subjected to blast loading, based on previous experimental results. For the sake of completeness, it is worth clarifying that the Nurick's number reported above is not the only number that has been proposed in the literature, but it is herein given a major insight since it is the only number considered in the present work. For instance, from the aforementioned analytical theory of Jones, a dimensionless number can be extracted, which allows predicting the permanent deflection-thickness ratio for dynamically loaded structures [14]. Since the two-part work by Nurick and Martin [17] [18], many analytical, experimental, and numerical studies of the response of structures to dynamic loading have been published. These investigations have expanded the existing theories to more types of structures, e.g., different plate geometries, stiffened and welded structures, sandwich panels, composite materials and monolithic metal plates with different boundary conditions. The interested reader is referred to the works in [19, 20, 21, 22, 23, 24, 25, 26] to get a deeper insight into some of these topics. In addition, different loading conditions have been assessed, including the effects of localised impulsive loading and those determined by changing the standoff distance. A paper intended as a literature review of the works published since 1989 was published in 2016 [27] to update the two-part work presented by Nurick and Martin. An updated version of the empirical formula introduced in [18], aimed at predicting the deflection-thickness ratio of quadrangular clamped plates on the basis of the Nurick's number ϕ, was proposed there, showing a good correlation with experimental results. Note, however, that the vast majority of the experimental results came from lab-scale tests, which involved the generation of an impulsive loading on the target plate by detonating plastic material near the plate itself. In particular, in case the standoff distance influence was not of interest, the plastic explosive was directly attached to the plate. Instead, two alternative techniques were adopted for increasing the standoff distance, i.e., either a layer of different material was interposed between the explosive and the plate, or the charge was placed on top of a bridge. It is worth noting that the former method, i.e., attaching explosive material directly onto the plate surface, certainly produced an impulsive loading on the target, even though the physical phenomena involved were different, in nature, from the ones governing the blast wave-structure interaction phenomenon. In this context, very few experimental studies have been performed which involve the large-scale detonation of explosive material. The work in [28] presented the results of two test programmes involving quadrangular mild steel plates subjected to pressure load from exploding charges, considering both compacted and widespread, i.e., carpet-like, layouts. The empirical predictions obtained applying the methodology presented in [27] to the tests in the experimental campaign did not always provide accurate results compared to the experimental measurements. The lack of accuracy was most likely due to the imperfect terrain and the complex explosive loading arrangement. Moreover, the impulse imparted to the plate was not measured experimentally, but only estimated employing consolidated empirical equations. However, in so doing, only the incident impulse, not the effective one exerted on the target, was considered to determine the Nurick's number value, which underestimated the load on the plates. In fact, as soon as a blast wave hits a structure, it is reflected in the impact event, giving rise to a reflected pressure wave, the combination of which with the incident wave determines the effective pressure exerted on the target. More recently, Xu et al. in the work in [29] investigated the behaviour of thin aluminium plates subjected to large-scale explosions. The dimensionless Nurick's number expression was modified, according to previous results reported in the work by Langdon et al. [30], introducing the Specific Energy To Fracture (SETF) value. The experimental results seemed to agree with the empirical relationship proposed in [18] for the only plates characterised by Mode I-A deformation, i.e., large permanent deflection with necking around part of the boundary, without any tearing. However, as already discussed above regarding the procedure adopted in the work in [28], the Nurick's number values were obtained considering the only incident impulse determined by the explosion as the impulse imparted to the plate. Few works have considered the effective impulse exerted on the impacted plate as the one driving the deflection of the impacted structure. Among them, the work in [31] compared numerical and analytical predictions to experimental observations of the permanent transverse displacement of square plates subjected to blast loading, showing good estimation capability both for hydrocode analyses in ANSYS® AUTODYN® and for the analytical theory proposed by Jones [15]. Finally, it is worth mentioning the works in [32, 33], which compared the results obtained using an Analytical-Lagrangian approach, exploiting the CONWEP analytical model to characterise the blast load, to experimental results. The works showed that the considered methodology provides fast and reliable results in estimating both the reflected blast pressure and the structural response. Moreover, the work in [33] also satisfactorily simulated plates undergoing counter-intuitive behaviour (CIB), providing results in good agreement with experimental observations [34], highlighting that the blast pressure negative phase plays a fundamental role in such a phenomenon. Another large-scale test was presented by Børvik et al. in the works in [35] and [36], involving the explosion of the equivalent of 4000 kg TNT at 120 m standoff distance from an unprotected 20 ft ISO container. The experimental setup, the blast characteristics measured during the test and the front panel maximum permanent transverse deflection observed were also presented there. In a subsequent work in [5], different types of numerical simulations of the event reported in the works [35] and [36] were presented, which seemed not to provide satisfactory predictions compared to the deflection measured in the full-scale experimental test. That was mainly due to the particular charge layout used for producing the blast wave, which determined a scenario not easily characterisable employing the explosion of an equivalent mass of TNT material. However, introducing the correction accounting for the measured impulse exerted on the structure, the numerical deflection estimation shifted towards the measured value, thus providing satisfactory results. However, no comparison to the Nurick's empirical equations ([18] [27]) was performed.

In the context outlined above, this paper aims at establishing a detailed comparison of the main fully analytical and empirical methods available in the literature, exploiting consolidated experimental evidence and results from numerical simulations. A similar work by Mostofi et al. [37] already compared analytical and empirical methods available in the literature, but it was limited to experimental observations only and it did not consider large-scale explosions. The focus of this work is only on the estimation of the permanent transverse deflection of a quadrangular, initially flat plate subjected to blast loading. Both close-range and far-field explosions are accounted for in the following. Moreover, a modelling framework is presented, which serves as a fast and reliable predictive tool to estimate blast load effects on plates. The framework is composed of two modules: the first module characterises the blast wave propagation and its interaction with the target structure analytically, this information is then transferred to the second module, which predicts the permanent transverse deflection of a quadrangular, initially flat plate.

This paper is organized as follows: Section 2 presents the main consolidated methods for the characterisation of the permanent transverse deflection of quadrangular, initially flat metal plates and introduces the modelling framework developed for the same purpose. Section 3 introduces the numerical simulations performed to build the database for the comparison of the selected methods, along with the database from experimental campaigns found in the literature. Section 4 reports a detailed comparison of the aforementioned selected predictive tools, including the software developed by the authors. Finally, Section 5 gives the conclusions and presents possible future work.

2 Main predictive methods

This Section aims at presenting the main fully analytical and empirical methods for estimating the permanent transverse deflection of plates in explosive scenarios. Two methods are selected from the ones present in the literature, namely the method proposed by Jones [15] and the dimensionless analysis from Nurick and Martin [17] [18] [27]. In particular, the comparison is focused on quadrangular metal plates subjected to close-range and far-field explosions. Moreover, the modelling framework developed within this work is introduced in this Section.

2.1 Jones's theory

Jones proposed in the work in [15] an exhaustive, fully analytical theory for characterising the permanent transverse deflection of arbitrarily shaped plates subjected to several types of loading, i.e., low-velocity impact by a solid mass, dynamic pressure pulse and impulsive velocity loading. The plate material was idealised as a rigid, perfectly plastic material and finite deformation effects, such as membrane forces and geometry changes, were retained in the analysis. Moreover, the influence of the material strain rate was taken into account employing the Cowper-Symonds constitutive equation [12], which provides an estimate of the dynamic flow stress as a function of some material-dependent parameters.

Considering an initially flat rectangular plate of length $2L$ and width $2B$, fully clamped at the edges and subjected to a uniformly distributed impulsive velocity V_0, the equation giving the deflection-thickness ratio is [31]:

$$\frac{W_f}{H} = \frac{(3-\xi_0)\left[\sqrt{1+\frac{\Gamma}{n}}-1\right]}{2\{1+(\xi_0-1)(\xi_0-2)\}} \tag{1}$$

where W_f is the permanent transverse central deflection, H is the plate thickness, while the remaining variables are analysed in the following. Defining the plate width to length ratio as $\beta = L/B$, it holds:

$$\xi_0 = \beta\left[\sqrt{3+\beta^2}-\beta\right] \tag{2}$$

$$\Gamma = \frac{2\rho V_0^2 L^2 \beta^2}{3n\sigma_0 H^2}(3-2\xi_0)\left(1-\xi_0+\frac{1}{2-\xi_0}\right) \tag{3}$$

where ρ and σ_0 are the plate material density and static yield stress, respectively. The strain rate effects are considered through the coefficient n:

$$\mathrm{n} = 1 + \sqrt[q]{\frac{V_0 H\,(3-\xi_0)\sqrt{\Gamma}}{6\sqrt{2\mathrm{D}}\mathrm{B}^2[1+(\xi_0-1)(\xi_0-2)]}} \tag{4}$$

Equation (4) introduces the Cowper-Simonds coefficients q and D. It is herein assumed that these coefficients are common to all the steel materials considered in this work, i.e., $q = 5$ and $D = 40.4\ s^{-1}$ from the values used in the work in [15] for mild steel, while they are neglected, i.e., the strain rate effect is not considered, in case of scenarios involving aluminium.

2.2 Nurick and Martin's dimensionless number

Unlike Jones, who carried out the relationships presented above through analytical considerations only, Nurick and Martin developed a fully empirical, experiment-based dimensionless analysis to deal with plates under blast loading [17]. This analysis provided a dimensionless number capable of estimating the deflection-thickness ratio of quadrangular or circular, initially flat metal plates, which was supposed to be valid for any metal material. Focusing on the uniform dynamic loading case, considering quadrangular plates fully clamped at the edges, the dimensionless number ϕ reads:

$$\phi = \frac{\hat{I}LB}{2H^2\sqrt{LB\rho\sigma_0}} \tag{5}$$

where $\hat{I}$ identifies the effective specific impulse imparted to the plate. Moreover, an empirical equation relating the dimensionless number value to the expected deflection-thickness ratio was also proposed by the authors of the method, based on model fitting to experimental results [27]:

$$\frac{\delta}{t} = 0.506\phi - 0.158 \tag{6}$$

This equation allows predicting the permanent transverse mid-point deflection of blast loaded quadrangular plates with a probability of 72% within one plate thickness and of 92% within two plate thicknesses [27]. Note that the Nurick and Martin's theory implicitly considers strain rate effects since equation (6) directly comes from experimental observations. However, since the experimental campaigns were mainly conducted on mild steel plates, an extension to other metal materials is not straightforward.

2.3 Modelling framework

The methods presented above are quite consolidated. However, to the authors' best knowledge, no practical implementation of such approaches has been pursued yet, even though that would allow providing a reliable preliminary predictive tool to instantaneously estimate the permanent transverse central deflection of arbitrarily shaped, initially flat metal plates. A possible reason why such tools have not been developed yet may be that they would require the characterisation of the impulse imparted by the blast wave to the impacted plate. This information may be provided exploiting hydrocode analyses or analytical characterisation tools, such as the CONWEP approach [38]. The former would lead to time- and resource-consuming analyses, hence it would not be suitable for integration into a framework aimed at providing fast and reliable preliminary predictions. On the other hand, blast wave analytical characterisation tools may be more suitable for that purpose. However, they are typically implemented in finite element commercial solutions, resulting in quicker analyses than hydrocode ones, exploiting the aforementioned Analytical-Lagrangian method, while still requiring greater computational resources than a fully analytical method.

In this context, a two-module modelling framework with both blast wave properties and permanent transverse central deflection of arbitrarily shaped, initially flat metal plates prediction capabilities is proposed. The *blast wave characterisation module* requires as input values (i) the charge location in space, (ii) the explosion type, i.e., hemispherical or free-field, (iii) the material the ground is composed of, if any, and (iv) the target structure material and exposed area properties. The module characterises the blast wave time history and propagation in space exploiting the modified Friedlander equation [39], the parameters of which are estimated employing consolidated empirical models present in the literature [40, 41, 42], while the blast wave-structure interaction phenomena are accounted for exploiting the theory included in the UFC 3-340-02 [41]. This successfully sets up a methodology that allows solving some typical issues of the CONWEP method, such as the wrong reflected pressure prediction in case of oblique impacts or the unsatisfactory blast wave-structure interaction characterisation. More information about the equations implemented in the blast wave characterisation module and the module validation analysis can be retrieved in the work in [43]. The blast wave characteristics and its interaction with the impacted plate are directly transferred to the *deflection prediction module*, which implements both the Jones' theory and the Nurick and Martin's dimensionless approach to predict the permanent transverse central deflection of the target plate. For the sake of clarity, it is recalled that in this work only quadrangular plates are considered. The software structure is shown in Figure 1.

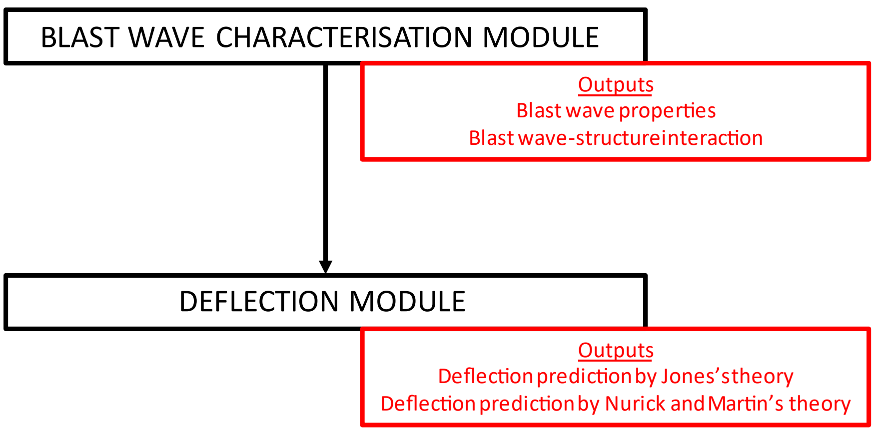

Figure 1. Modelling framework structure.

3 Database

A database including both experimental and numerical results is built to compare the selected approaches, i.e., the Jones' theory and the Nurick and Martin's dimensionless analysis. While experimental results are taken from the quite ample literature available on the topic, numerical results are gained employing Analytical-Lagrangian analyses and fully coupled Eulerian-Lagrangian simulations, i.e., hydrocode simulations. In this Section, the procedure employed for performing such numerical analyses is presented and the whole database introduced. Numerical simulations are performed in LS-DYNA® and in ANSYS® AUTODYN®. These software packages implement several methods to analyse structures subjected to blast loading. In this work, the former software is exploited to perform Analytical-Lagrangian analyses, while the latter is involved in the Eulerian-Lagrangian simulations.

3.1 Analytical-Lagrangian numerical analysis setup

The analytical characterisation of the blast wave propagation and interaction with the target structure implemented in LS-DYNA® employs the CONWEP approach [7], a consolidated method which is based on the Kingery and Bulmash equations, which were obtained via model fitting to a large number of experimental results [44]. The main variable involved in the equations is the scaled distance Z, coming from the scaling law independently formulated by Hopkinson [45] and Cranz [46], which is defined as:

$$Z = \frac{R}{\sqrt[3]{W_{TNT}}} \tag{7}$$

where R is the distance of the point of interest from the detonation location and W_{TNT} the TNT equivalent weight of the explosive involved in the detonation. The reader is referred to chapter 3 of the work in [47] for further information on the TNT equivalent weight topic. It is noteworthy that CONWEP equations hardly deal with oblique impacts and only provide an approximated value of the pressure-time history exerted on the target structure, without accounting for the finite dimensions of the latter [43]. For this reason, only normal impacts are herein assessed employing this approach, considering the slightly inaccurate blast wave-structure interaction characterisation a minor issue. Moreover, only free-field and hemispherical explosions, i.e., in air and on-the-ground explosions, respectively, are simulated, neglecting the blast wave negative phase effects, since they are not of great importance for the target structure damaging process in the scenarios considered in this work [41] [40].

The effective pressure-time history exerted on the impacted plate, as determined via the CONWEP method, is applied to the plate finite element model. The plates considered in the analyses are all fully clamped at the edges, the boundary conditions are applied in a simplified way, exploiting a single point constraint at each node belonging to the plate exposed area edges. The material constitutive law selected to model steel and aluminium is the modified Johnson-Cook constitutive law (MJC) shown in equation (8), which allows considering the effects of high strain rate, large plastic deformation and high temperature typical of the scenarios considered herein [48, 49]. In this equation, the material constant A represents the elastic limit, B and n describe the plastic behaviour and hardening, c the strain rate influence, m the temperature influence, while Q_i and C_i represent the Voce hardening parameters. Moreover, ε_{eq} is the equivalent plastic strain and T^* the dimensionless temperature.

$$\sigma_{eq} = \left[A + B\varepsilon_{eq}^{n} + \sum_{i=1}^{2} Q_i\left(1 - e^{-C_i\varepsilon_{eq}}\right)\right]\left(1 + \dot{\varepsilon}_{eq}^{*}\right)^{c}\left(1 - T^{*m}\right) \tag{8}$$

The constitutive law parameters and the physical constants for the materials considered in the analyses are reported in Table 1 and in Table 2, respectively, where $\sigma_{0.2}$ represents the yield stress, $\dot{\varepsilon}_0$ the reference quasi-static strain rate, T_r the reference temperature and T_m the melting temperature. Note that for Mild Steel the strain rate influence is accounted for employing the classical Johnson-Cook relationship, i.e., $\left(1 + c\,ln\dot{\varepsilon}_{eq}^{*}\right)$ instead of the term $\left(1 + \dot{\varepsilon}_{eq}^{*}\right)^{c}$ in equation (8) [50].

Material	$\sigma_{0.2}\ [MPa]$	$A\ [MPa]$	$B\ [MPa]$	n	$Q_1\ [MPa]$	C_1	$Q_2\ [MPa]$	C_2	c	$\dot{\varepsilon}_0 [s^{-1}]$	$T_r\ [K]$	$T_m\ [K]$	m	Ref
Mild Steel	304.3	304.3	422.0	0.345	0.0	0.0	0.0	0.0	0.0156	1×10^{-4}	293	1800	0.87	[51]
Weldox 500E	605.0	605.0	409.0	0.5	0.0	0.0	0.0	0.0	0.0166	5×10^{-4}	293	1800	1.00	[48]
Weldox 700E	819.0	819.0	308.0	0.64	0.0	0.0	0.0	0.0	0.0098	5×10^{-4}	293	1800	1.00	[48]
Hardox 400	1148.0	1350.0	362.0	1.0	0.0	0.0	0.0	0.0	0.0108	5×10^{-4}	293	1800	1.00	[48]
Docol 600DL	370.0	370.0	0.0	0.0	236.4	39.3	408.1	4.5	0.001	5×10^{-4}	293	1800	1.00	[33]
1050A H14	80.0	80.0	0.0	0.0	49.3	1457.1	5.2	121.5	0.014	5×10^{-4}	293	893	1.00	[33]
1050A H24	65.0	65.0	14.0	0.36	25.0	3324.0	19.0	533.0	0.014	5×10^{-4}	293	918	1.00	[52]

Table 1. MJC constitutive law parameters for the materials.

Material	$E[GPa]$	ν	$\rho\ [kg/m^3]$	$\alpha\ [1/K]$	$C_P [J/kgK]$	χ	Ref
Mild Steel	203	0.33	7850	1.2×10^{-5}	452	0.9	[51]
Weldox 500E	210	0.33	7850	1.2×10^{-5}	452	0.9	[48]
Weldox 700E	210	0.33	7850	1.2×10^{-5}	452	0.9	[48]
Hardox 400	210	0.33	7850	1.2×10^{-5}	452	0.9	[48]
Docol 600DL	210	0.33	7850	1.2×10^{-5}	452	0.9	[33, 34]
1050A H14	70	0.3	2700	2.3×10^{-5}	910	0.9	[33, 34]
1050A H24	69	0.33	2710	2.3×10^{-5}	899	0.9	[32, 52]

Table 2. Physical constants for the materials.

The plate model is composed of *hexahedral solid elements* with formulation *elform-1*, which is an efficient fully integrated formulation limiting the shear-locking effect intended for elements with a poor aspect ratio, thus being suitable for the analysis of thin panels subjected to dynamic loading. Convergence analyses show that the appropriate element dimensions in the plate plane are at least $5.56\ \mathrm{mm}$ x $5.56\ \mathrm{mm}$, while a maximum of $1.5\ \mathrm{mm}$ is required in the plate thickness. Table 3 reports the results of some of the analyses conducted for the convergence evaluation, which involve the detonation of a 1135.2 kg spherical TNT charge at 13.35 m from a $3\mathrm{mm}$ thick Weldox 500E plate with an exposed area of $500\mathrm{mm}$ x $500\mathrm{mm}$. This particular combination of stand-off distance and explosive mass is part of the database considered in this work, which is reported below in Table 10. All the element dimensions considered in Table 3 guarantee convergence since they provide results with a negligible error with respect to the immediately larger mesh size tested.

Element type	Mesh size [mm]	Permanent deflection [mm]	Error with respect to the previous size
Solid elform-1	6.25 x 6.25 x 1	34.8	~
Solid elform-1	6.25 x 6.25 x 0.75	34.8	0%
Solid elform-1	5.56 x 5.56 x 3	34.7	-0.3%
Solid elform-1	5.56 x 5.56 x 1.5	34.9	0.6%
Solid elform-1	5 x 5 x 1.5	34.8	-0.3%

Table 3. Analytical-Lagrangian convergence analysis results.

Global viscous damping is added to the analyses to stop elastic oscillations that may alter the detection of the maximum permanent deflection of the central point of the target panel [53]. To this purpose, the card *DAMPING_GLOBAL is activated, which defines mass-weighted nodal damping that applies globally to the nodes of deformable bodies and to the mass centre of rigid bodies according to:

$$\vec{F}_{d,i} = -m_i \vec{v}_i D_s \tag{9}$$

where $\vec{F}_{d,i}$ is the force applied to the i-th node, m_i the mass attributed to it, $\vec{v}_i$ its velocity and D_s the damping coefficient. A value of 10% of the critical damping $2\omega_{min}$ is typical for D_s [54], which is defined as:

$$D_s = \frac{2\omega_{min}}{10} = \frac{2 \cdot 2\pi f_{min}}{10} = 0.4 \cdot \pi f_{min} \tag{10}$$

where f_{min} is the frequency of the lowest frequency fundamental mode of the structure, which in this work is determined performing the eigenvalue analysis of the structure itself using the LS-DYNA® implicit solver. The damping forces are activated once the blast load acting on the panel becomes null, which is needed not to alter the deformation process of the structure when the pressure exerted on the target has not vanished yet. Finally, in order to recover the central transverse permanent deflection of the plate, the displacement-time signal of the central front node of the finite element model is post-processed. The maximum frequency excited by the blast wave impacting the target (f_c) is identified as that value of frequency at which the unilateral spectrum modulus of the effective pressure exerted on the target is reduced to 10% of the maximum registered pressure:

$$f_c = f \mid \overline{FFT}_{pressure}(f) = 0.1 \cdot \max\left(\overline{FFT}_{pressure}\right) \tag{11}$$

where $\overline{FFT}_{pressure}(f)$ identifies the unilateral spectrum modulus of the effective pressure-time history. The value f_c is set as the cut-off frequency of a Butterworth low-pass filter, which is applied to cancel out the numerical noise affecting the considered displacement-time curve. The final step consists of taking the mean value of the panel central point deflection data when the plasticisation transient is finished, which is needed since damping may not be able to completely eliminate the lasting elastic oscillations of the panel. This process may be avoided by incrementing the time duration of the damping forces exerted on the nodes of the structure, but that would significantly slow down the analysis. The whole post-processing procedure is schematised in Figure 2.

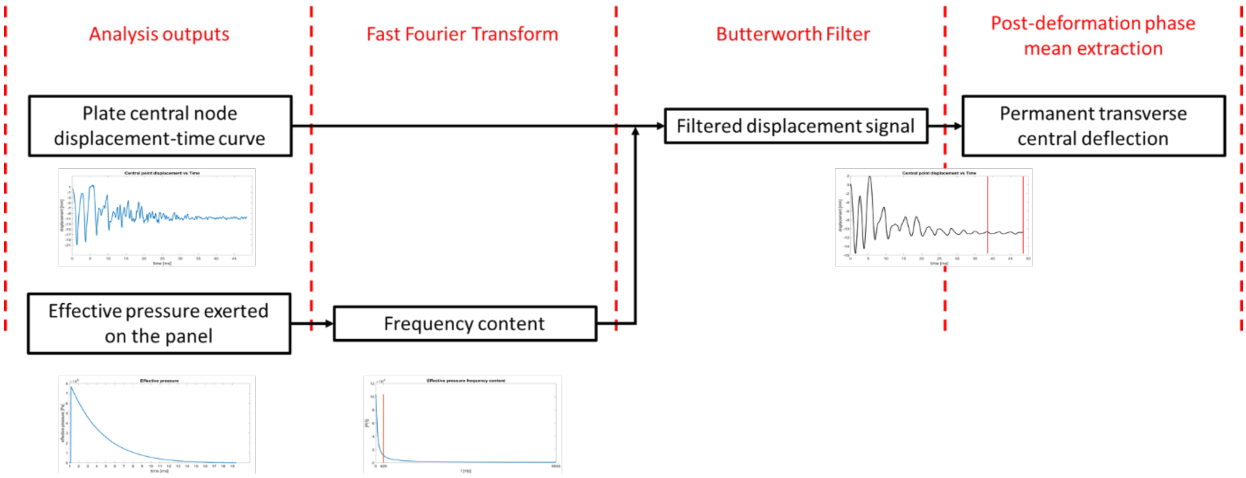

Figure 2. Plate central node displacement signal post-processing procedure.

3.2 Fully coupled Eulerian-Lagrangian numerical analysis setup

Fully coupled Eulerian-Lagrangian analyses, or hydrocode analyses, are performed within the finite element ANSYS® AUTODYN® environment. The analyses consist of the simulation of the formation and propagation of the compression wave inside the high explosive material, which determines a shock wave that propagates in air, evolves in time and space and eventually hits a surrounding structure. Lagrangian grids are exploited to model the target structure, while air and TNT are described through Eulerian grids. The former provide the geometry constraint for the material flow in the Eulerian grids, which in turn provide a pressure and/or heat boundary to the Lagrangian domain. AUTODYN® allows using different solvers for the different domains in the simulation. In this work, the Lagrange solver deals with the plate deformation, while the air domain is set up using the

Euler-Godunov solver, the explosive material is set in the air domain. Moreover, the domains in the analysis are coupled together in space and time. Within the Euler solver, AUTODYN® adopts a scheme in which all the variables, e.g., pressure and energy, are cell centred, which facilitates coupling procedures [55]. The software package includes three types of Euler/Lagrange coupling, i.e., Rigid, Weak coupling and Fully coupled. The latter is selected in the hydrocode analyses presented in this work.

In order to lower the time and resources consumption, thanks to the spherical charge layout considered in this work, symmetry is exploited for characterising the blast wave. In fact, the phenomena taking place within the sphere are independent of the circular section considered. Moreover, within each circular section the wave characteristics are independent of the angular sector considered. Thus, the analysis is initially performed considering a 2D angular sector, which is further remapped in the 3D space before the blast wave strikes the target structure.

The explosive material behaviour is modelled employing the JWL EOS [6], which is shown in equation (12), while the material in which the developed blast wave propagates, i.e., air in this work, is assigned the ideal gas EOS [56] (equation (13)). In the two EOSs, P represents the pressure, V the inverse of density ρ and e the material internal energy. More specifically, in the JWL equation ω stands for the Grüneisen coefficient, A and B are parameters with pressure units, R_1 and R_2 are dimensionless parameters. In the ideal gas EOS, γ represents the adiabatic constant and p_{shift} the small initial pressure value defined to give a zero-starting pressure. The default parameters included in the AUTODYN® database, which are shown in Table 4 and Table 5, are selected for the two equations of state. Detonation is initiated by positioning the detonation point at the centre of the sphere describing the explosive material.

$$P(V,e) = A\left[1-\frac{\omega\cdot V_0}{V\cdot R_1}\right]\cdot e^{-\frac{V\cdot R_1}{V_0}} + B\left[1-\frac{\omega\cdot V_0}{V\cdot R_2}\right]\cdot e^{-\frac{V\cdot R_2}{V_0}} + \frac{\omega}{V}(e+\Delta e) \tag{12}$$

$$P = (\gamma-1)\cdot\rho\cdot e - p_{shift} \tag{13}$$

Material	$A\ [MPa]$	$B\ [MPa]$	R_1	R_2	ω	$\rho_0 [kg/m^3]$
TNT	$3.7377\cdot 10^5$	$3.7471\cdot 10^5$	4.15	0.9	0.35	1630

Table 4. JWL equation of state parameters [57].

Material	$\rho_0\ [\mathrm{kg}/m^3]$	γ	Ref. Temperature [K]

Air	1.225	1.4	288.2

Table 5. Ideal gas equation of state parameters [57].

The distal boundary of the angular sector filled with TNT and air is assigned the *Flow-out* boundary condition, which lets the blast wave go through without any undesired reflection. The angular sector is meshed with Eulerian cells of regular geometry, the dimension of which is determined through the convergence analysis described below, which involves the detonation of $1\ \mathrm{kg}$ of TNT. The peak overpressure value is obtained by positioning a virtual pressure gauge at $0.5\ \mathrm{m}$ distance from the detonation point, hence $\mathrm{Z} = 0.5\ \mathrm{m/kg^{1/3}}$.

Cell size [mm]	**Peak overpressure [MPa]**	**Error with respect to the previous size**
5	2.992	~
2.5	3.329	11%
1	3.134	-6%
0.25	2.922	-7%

Table 6. Hydrocode convergence analysis results.

Convergence is assessed by evaluating the error in the peak overpressure value: the cell dimension which guarantees convergence is considered to be the one that provides the results with an absolute value error with respect to the immediately larger mesh size tested lower than 10%. The cell size of $1mm$ is selected, which implies a computational time of about one hour per convergence analysis.

The size of the Lagrangian elements exploited for characterising the target structure behaviour meet the convergence requirement described in Subsection 3.1. Moreover, the adopted dimensions are also compatible with the requirement that Lagrangian cell size should be at least two times that of the adjacent Eulerian cells, considering the coupling scheme exploited in the analysis [58]. The material constitutive law selected in the simulations is the Johnson-Cook constitutive law, integrated with the Mie–Grüneisen equation of state (shock EOS) [59] to determine the volumetric response of the material itself. The default parameters for mild steel in the database of ANSYS® AUTODYN® (Table 7, Table 8) are selected in the analyses. Fully clamped boundary conditions are set up imposing zero velocity at the plate exposed area edges.

Material	$G\ [MPa]$	$A\ [MPa]$	$B\ [MPa]$	C	n	$T_{melt}\ [K]$	m
Mild steel	$8.18 \cdot 10^4$	350	275	0.022	0.36	1811	1

Table 7. Mild steel JC constitutive law parameters [57].

Material	Γ	$C_1\ [m/s]$	S_1	$C_2\ [s/m]$
Mild steel	2.17	4569	1.49	0

Table 8. Mild steel Shock EOS parameters [57].

3.3 Database

In order to compare the selected predictive methods, a database of scenarios available in the literature is set up. Some of these scenarios are simulated numerically, exploiting Analytical-Lagrangian analyses, while all of them are characterised employing the analytical theories considered in this work. Moreover, whenever the experimental mid-point permanent deflection is available, it is compared to the simulation results. Large scale explosions are inspired by the experimental campaign described in the work in [28], where quadrangular mild steel plates are subjected to pressure loads determined by exploding charges both in compacted and in carpet-like form, producing hemispherical detonations. Moreover, these scenarios are numerically extended by simulating free-field detonations of the same explosive charges, considering quadrangular plates made of mild steel and ballistic steels, such as Weldox 500E, Weldox 700E and Hardox 400 as test structures. Mild steel is also used in the works in [5] and in [31], while low carbon steel, i.e., Docol 600DL, is considered in the works in [33, 34]. All of these scenarios are included in the database. Moreover, some tests on aluminium plates are also evaluated in this work, i.e., the analyses presented in the works in [32, 33, 34]. The whole database considered in this work is reported in Table 9, where the letters E, A and N stand for Experimental, Analytical and Numerical (Analytical-Lagrangian), respectively. The analytical and numerical analyses are performed by the authors, while the experimental results are taken directly from the referenced works.

Analysis code	Materials	Explosion type	Analyses	Reference
Vastrap - Hemispherical (V-H)	Mild steel	Hemispherical	E, A	[28]
Touwsrivier - Hemispherical (T-H)	Mild steel	Hemispherical	E, A	[28]
Vastrap - Free-field (V-F)	Mild steel, Weldox 500E, Weldox 700E, Hardox 400	Free-Field	A, N	[28]
Touwsrivier – Free-field (T-F)	Mild steel, Weldox 500E, Weldox 700E, Hardox 400	Free-Field	A, N	[28]
Børvik – Hemispherical (B-H)	Mild steel	Hemispherical	E, A	[5]
Safari – Free-field (Sa-F)	Mild steel	Free-Field	E, A, N	[31]
Spranghers – Free-field (Sp-F)	1050A H24	Free-Field	E, A, N	[32]
Aune – Free-field (A-F-S)	Docol 600DL	Free-Field	E, A, N	[33, 34]
Aune – Free-field (A-F-A)	1050A H14	Free-Field	E, A, N	[33, 34]

Table 9. Database considered in this work. E: Experimental, A: Analytical, N: Numerical.

The scenarios evaluated in each analysis code reported above are presented in the next table. The *Plate dimensions* column presents the plate exposed area and thickness in the form *Height x Width x Thickness*, the *Amount of explosive* column reports the TNT equivalent weight of the actual explosive considered. Note that, in case of hemispherical explosions (H), the scaled distance value is computed considering a TNT amount obtained multiplying the one reported in the table by a factor of 1.8, which aims at considering the effect of the blast wave strengthening due to the ground reflection. In the last column the radial expansion of the shock front at the plate location ($\bar{r}_{plate}$) is reported, which is determined as the ratio between the *Distance of explosion* value and the charge radius value, the latter computed as the radius of a sphere of mass *Amount of explosive* and density given in Table 4. This parameter allows identifying close-range explosions, which are characterised by $1 < \bar{r}_{plate} \leq 10$ [60].

Scenario code	Plate dimensions [mm]	Amount of explosive [kg]	Distance of explosion [m]	Scaled distance $[m/kg^{1/3}]$	$\bar{r}_{plate}$
V-F1 / V-H1	500x500x3	1119.8	18.0	1.73 / 1.43	32.9
V-F2 / V-H2	500x500x3	1119.8	22.5	2.17 / 1.78	41.1
V-F3 / V-H3	500x500x3	1119.8	19.5	1.88 / 1.54	35.6
V-F4 / V-H4	500x500x3	1135.2	13.35	1.28 / 1.05	24.3
V-F5 / V-H5	500x500x3	1135.2	12.25	1.17 / 0.97	22.3
V-F6 / V-H6	500x500x6	1119.8	18.5	1.78 / 1.46	33.8
T-F1 / T-H1	500x500x6	120.0	10.8	2.19 / 1.80	41.5
T-F2 / T-H2	500x500x6	190.0	9.3	1.62 / 1.33	30.7
T-F3 / T-H3	500x500x6	190.0	12.05	2.10 / 1.72	39.8
T-F4 / T-H4	500x500x6	190.0	14.35	2.50 / 2.20	47.4
B-H1	2500x6000x2	4000.0	120.0	6.21	143.4
Sa-F1	180x180x1	0.039	0.2	0.59	11.2
Sa-F2	180x180x1	0.181	0.25	0.442	8.4
Sa-F3	180x180x1	0.156	0.2	0.371	7.0
Sa-F4	180x180x1	0.195	0.2	0.345	6.5
Sa-F5	180x180x1	0.300	0.25	0.373	7.1
Sa-F6	180x180x1	0.277	0.2	0.307	5.8
Sa-F7	180x180x1	0.312	0.2	0.295	5.6
Sp-F1	300x300x3	0.054	0.25	0.663	12.5
A-F-S1	300x300X0.8	0.0402	0.125	0.36	6.9
A-F-S2	300x300X0.8	0.0402	0.250	0.73	13.8
A-F-A1	300x300X0.8	0.0402	0.375	1.09	20.8
A-F-A2	300x300X0.8	0.0402	0.500	1.46	27.7

Table 10. Scenarios considered in the analyses database.

The analytical methods considered in this work to predict the permanent deflection-thickness ratio of flat quadrangular plates were developed to deal with impulsive loading [15, 17, 18, 27]. The impulsive nature of the blast loads considered herein is verified, but not reported for the sake of brevity. It turns out that most of the scenarios presented in Table 10 are safely representable as impulsive loading, while V-F6, T-H4 and the analyses coded T-F deserve a deeper investigation, in particular when dealing with the material Hardox 400. However, since all these analyses are similar to each other and in the work in [27] T-H4 was considered impulsive, given that every other approximated load history which may be dealt with using analytical theories, e.g., rectangular pulse, appear not to apply to these load cases, these critical analyses are included in the database.

4 Comparison of the selected methods

4.1 Numerical procedure validation

The results from the analyses conducted in this work are discussed in this Section, after the validation of the numerical results. The validation procedure is performed for the Analytical-Lagrangian numerical simulations exploiting the scenario coded as Sp-F1 in the database reported in Table 10, while the scenario Sa-F1 is involved in the Hydrocode simulations validation. The experimental and the numerical results from the Analytical-Lagrangian and Hydrocode simulations performed in this work are reported in Table 11.

Analysis	Mid-point permanent deflection – thickness ratio	
	Sa-F1	Sp-F1
Experimental	11.7	7.3
Lagrangian	~	7.1
Hydrocode	12.4	~
|% error|	5.9%	2.7%

Table 11. Numerical analyses validation.

Since the percentage errors, which are computed taking the experimental value as the reference value, are negligible, the numerical results are considered validated. Note that in the Sp-F1 scenario the same experiment is conducted more than once in the work in [32] leading to the experimental mid-point permanent deflection-thickness ratio mean value reported in Table 11.

4.2 Results

The results of the analytical and numerical analyses performed are presented herein. Each mid-point permanent deflection-thickness ratio (δ/t) predicted in the analyses is classified according to the related dimensionless number ϕ. This number is computed considering the analytical specific impulse determined by the framework described in Section 2.3 for the analytical and experimental results, while the number related to each Analytical-Lagrangian analysis directly comes from the numerical specific impulse measured at the centre of the plate.

The results from all the experimental, analytical and Analytical-Lagrangian evaluations are reported in Figure 3. The analytical methods applied are the Jones' theory and the Nurick and Martin's method, respectively described in Subsections 2.1 and 2.2. Note, however, that two predictions per scenario are presented based on the Jones' theory acting as lower (LB) and upper bounds (UB) for an admissible range of deflection-thickness ratio. They are derived from the theory presented in Subsection 2.1, exploiting two maximum normal stress yield conditions, i.e., adopting the circumscribing and inscribing square yield conditions, respectively [15].

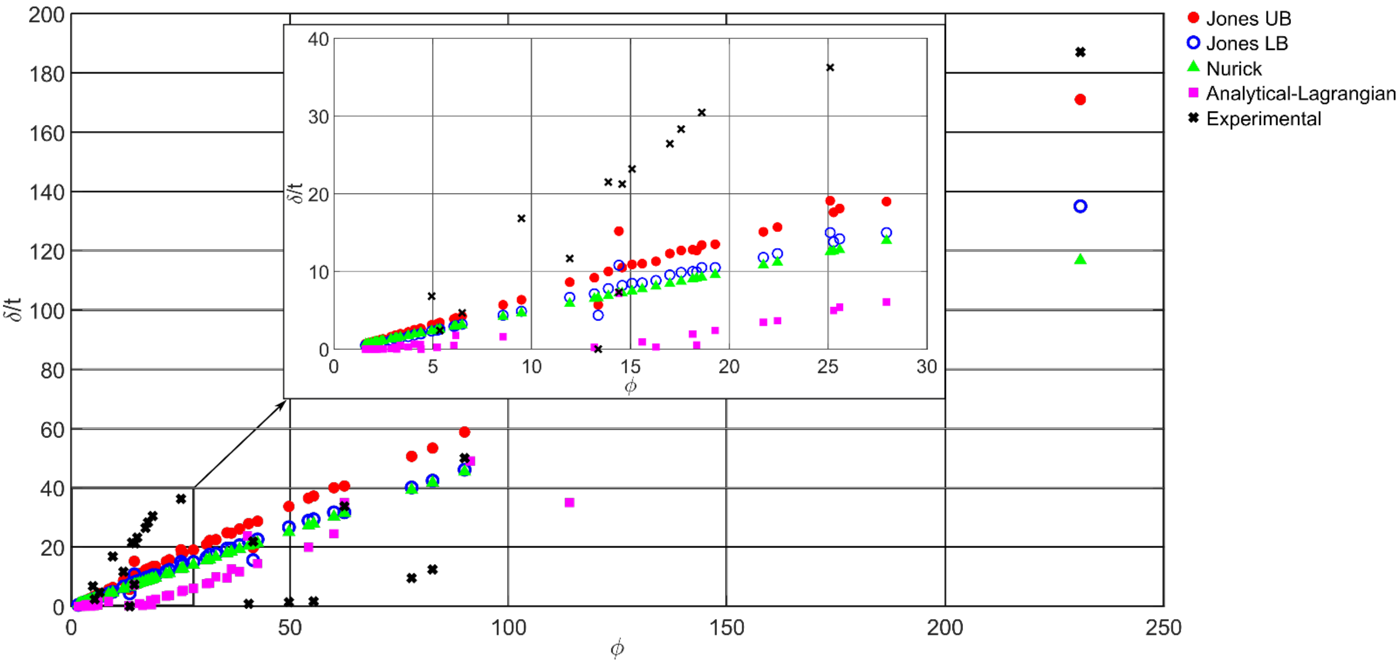

Figure 3. Results from all the experimental, analytical and Analytical-Lagrangian analyses.

As it is visible in this initial comparison, no overall agreement in the prediction of the value δ/t is obtained. However, considering the smallest dimensionless numbers computed, i.e., from 0 to 12, as shown in the zoom box in Figure 3, the analytical methods provide satisfactory results compared to the experimental observations, while the Analytical-Lagrangian simulations underestimate the predictions. At greater dimensionless number values, i.e., from $\phi = 12$ to $\phi = 30$, the analytical and numerical predictions seem to underestimate the δ/t ratio values with respect to the experimental observations, except for the scenario Sp-F1 at $\phi \cong 15$, for which the Jones' theory overestimates the experimental prediction. This might be related to the fact that this scenario involves an aluminium plate, for which the Cowper-Simonds coefficients are not considered, as already stated in Section 2.1. Instead, the ratio values are generally overestimated in the range from $\phi = 30$ to $\phi = 100$, with only few exceptions, which are correctly predicted. This overestimation may be determined by the fact that all the unsatisfactorily predicted experimental results in the range come from the scenarios coded as V-H in Table 9, which are the only ones in which a non-compacted charge layout was used. Hence, the dimensionless numbers associated with these experimental observations may be overestimated, since a carpet-like layout produces a weaker blast wave than the classical compacted layout [28]. In the work in [28] a different scaling law is suggested for this particular charge layout, i.e., $Z = R/\sqrt[4]{W_{TNT}}$. The use of this scaling law leads to the prediction of a lower impulse imparted to the structure and a lower associated dimensionless number ϕ, as it is shown in Figure 4. Note that in the figure the points related to the scenarios V-H are shifted according to the results obtained exploiting the updated scaled distance value.

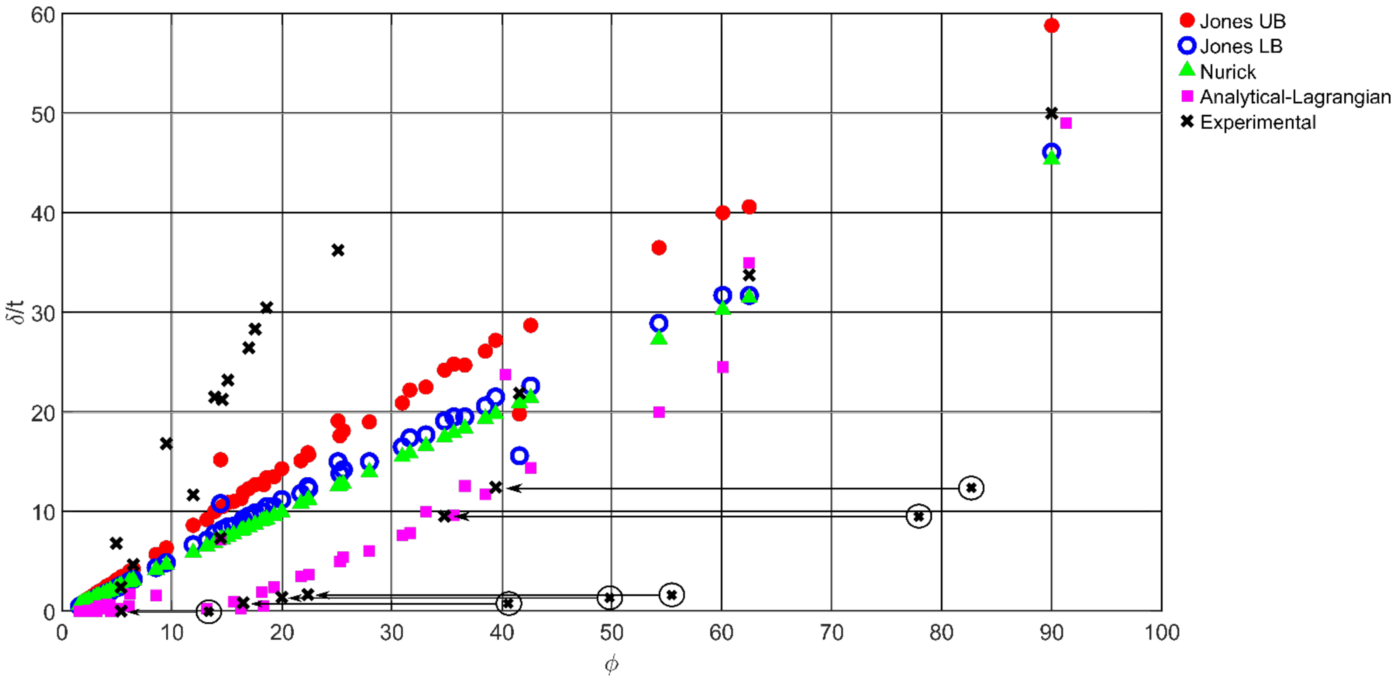

Figure 4. Results from all the experimental, analytical and Analytical-Lagrangian analyses – Carpet-like charge layout correction.

The experimental results presented in Figure 4 form three distinctive subsets, which are clearly outlined in Figure 5: the curve built employing Analytical-Lagrangian numerical analyses, identified by purple square markers, may be adopted for describing a subset of experimental results (SUB1), the curves from the Jones' theory and the curves built according to the empirical relationship from Nurick and Martin seem to provide a good estimate of the δ/t value for some other observations (SUB2), while no method considered in this work seems to be able to predict the points included in SUB3.

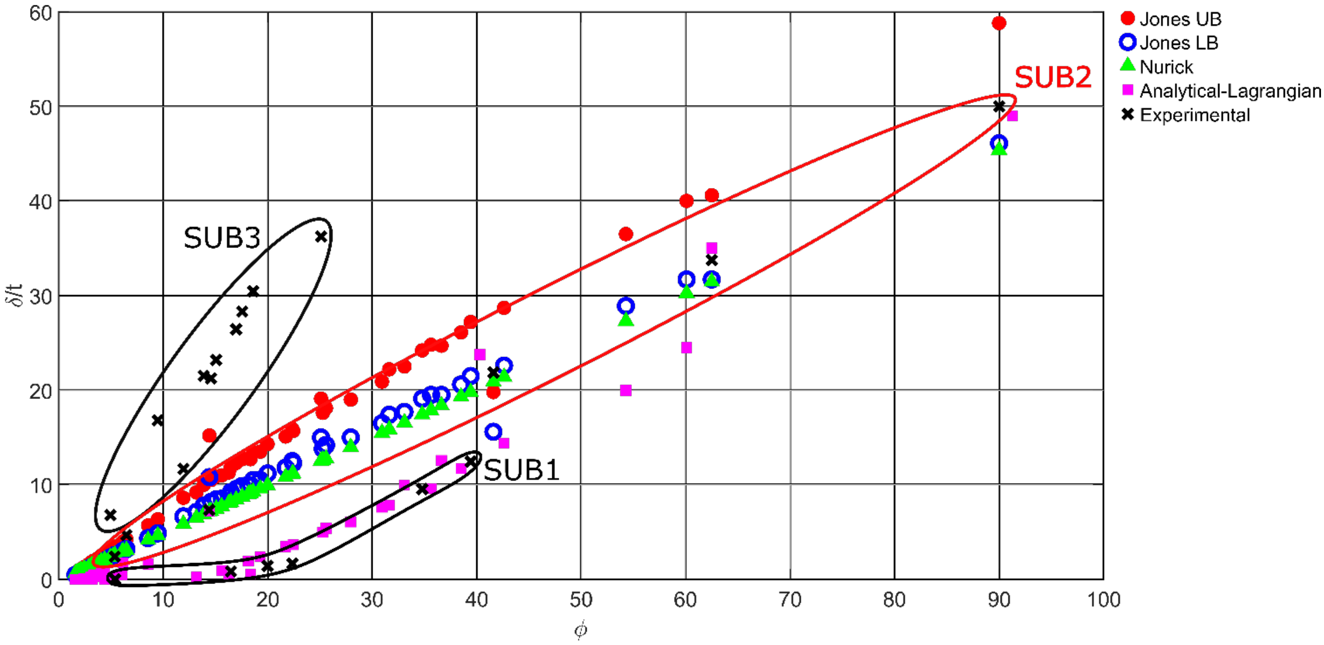

Figure 5. Identified data subsets.

The scenarios corresponding to the experimental results pertaining to each subset are reported in Table 12. The experimental observation B-H1 is not considered herein, since it is characterised by a dimensionless number way greater than the ones involved in all the other experimental campaigns.

SUB1	SUB2	SUB3
V-H1	T-H1	T-H2
V-H2	T-H3	T-H4
V-H3	Sp-F1	Sa-F1
V-H4	A-F-S2	Sa-F2
V-H5	A-F-A1	Sa-F3
V-H6	A-F-A2	Sa-F4
		Sa-F5
		Sa-F6
		Sa-F7
		A-F-S1

Table 12. Scenarios within the identified subsets.

It is worth highlighting that most of the scenarios identified in the subset SUB3, which is the one not predictable by the methods compared in this work, are characterised by small scaled distance values, i.e., $Z < 0.6 m/kg^{1/3}$, and small radial expansion of the shock front at the plate location, i.e., $\bar{r}_{plate} < 10$. These considerations suggest that (i) the impulse imparted to the structure may be inaccurately estimated, given the small scaled distance values [43], and that (ii) the underlying physics in close-range detonations, such as afterburning effect and fireball-interaction [60, 61, 62], should be taken into account when dealing with these scenarios. However, this is not possible using the methods involved to build the database, i.e., analytical and Analytical-Lagrangian analyses. Even though the previous considerations are not strictly valid for the scenario Sa-F1, it is characterised by a $\bar{r}$ value at the plate location slightly above the close-range limit, i.e., $\bar{r}_{plate} = 11.2$, which allows assuming close-range phenomena may still be relevant. Instead, the same considerations do not hold for the two scenarios of the T-H campaign, i.e., T-H2 and T-H4. However, in these scenarios the dimensionless number value may not be accurate enough as well, since the impulse imparted to the structure is estimated according to the procedure reported in Section 2.3, which is valid for spherical charges, while the real charge layout was non-spherical. These may be some possible reasons why no analytical method and Analytical-Lagrangian numerical method is able to predict the mid-point permanent deflection in such scenarios.

Differently, the experimental points included in the subset SUB2 can be described with the analytical methods compared in this work. It is worth noting that the three scenarios belonging to the A-F campaign and the scenario Sp-F1 are characterised by radial expansion of the shock front values at the plate location in the range $[12.5, 27.7]$, which classify those configurations as far-field configurations characterised by limited $\bar{r}_{plate}$ values. These scenarios are also satisfactorily characterised by the Analytical-Lagrangian analyses. The same considerations do not hold for the two scenarios of the T-H campaign, i.e., T-H1 and T-H3, which may be in this subset by chance.

Interestingly, all the experimental points included in the subset SUB1 are from hemispherical explosions involving a carpet-like charge layout. The only Analytical-Lagrangian curve seems to be able to characterise those explosive events, given that the dimensionless number associated with this particular charge layout is built up considering the modified scaled distance suggested in the work in [28], i.e., $Z = R/\sqrt[4]{W_{TNT}}$. Note, as a further remark, that the Analytical-Lagrangian numerical analyses describing the curve on which SUB1 is placed are performed considering free-field explosions only.

Hence, linear regression is performed considering the numerical curve to provide a predictive tool for explosions similar to the ones included in SUB1. To this purpose, only the results of the scenarios coded V-F and T-F are retained in the analysis, neglecting the ones related to Sp-F, A-F-S and A-F-A, which appear not to lie on the same curve. Only the points characterised by dimensionless number $\phi > 10$ are considered in the regression since the dispersion of the results below this threshold does not show an interpretable trend. The equation, which provides an R^2 value of 0.9881, reads:

$$\frac{\delta}{t} = 0.5227 \cdot \phi - 7.946 \qquad (14)$$

Thus, free-field explosions may be well approximated with the following bilinear curve:

$$\begin{cases} \frac{\delta}{t} = 0.5227 \cdot \phi - 7.946 \; for \; \phi \geq 15.2018 \\ \frac{\delta}{t} = 0 \qquad\qquad\qquad\quad for \; \phi < 15.2018 \end{cases} \tag{15}$$

Alternatively, a second-order polynomial may be exploited to provide a predictive equation for the experimental results in the subset SUB1. The curve fitting procedure, which is performed considering all the point in the numerical curve except the scenarios Sp-F, A-F-S and A-F-A, outputs with an R^2 value of 0.9594 (Figure 6):

$$\frac{\delta}{t} = 0.006149 \cdot \phi^2 + 0.05067 \cdot \phi \tag{16}$$

It is worth noting that, differently from the consolidated analytical methods described in this work, the provided equations allow predicting a null or negligible permanent deflection-thickness value for a range of small dimensionless numbers ϕ. This is judged to be a physically-sound result, since only completely elastic phenomena may occur in case low impulses are imparted to the plate. The Analytical-Lagrangian points considered are obtained with different types of steels (see Table 9), therefore, with a high confidence level, the regression curves proposed in this work may be valid for the whole steel materials category.

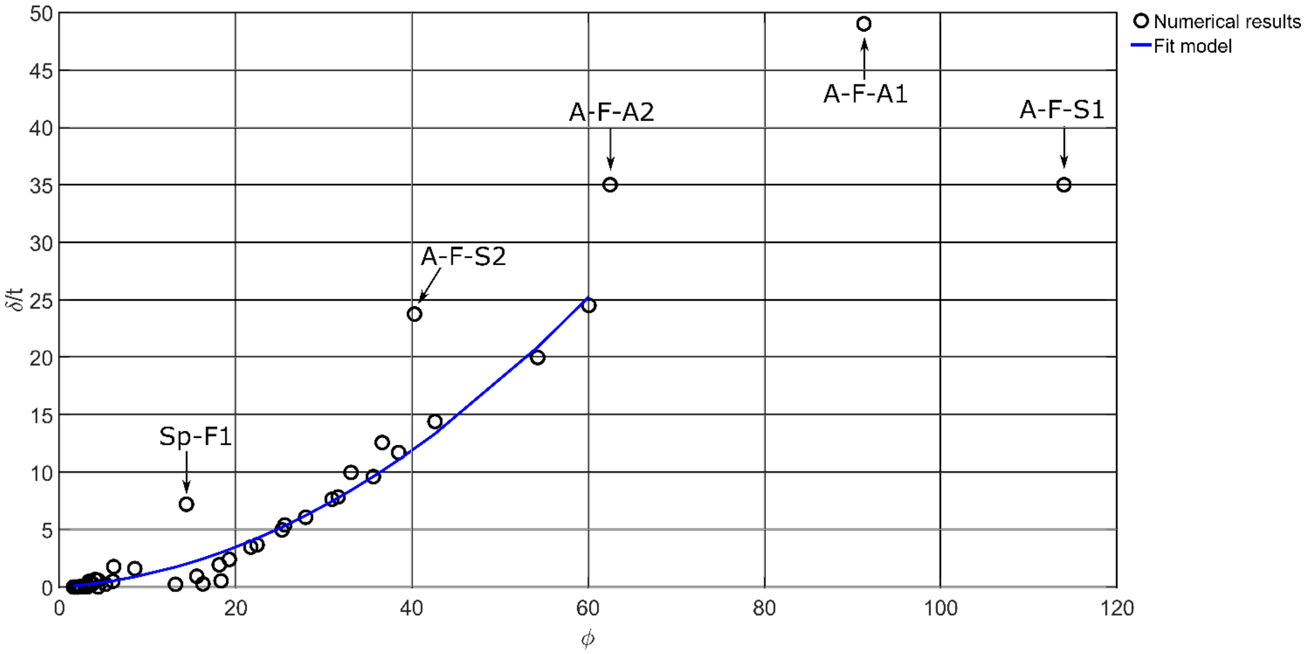

Figure 6. Regression on Analytical-Lagrangian analyses results with a second-order polynomial.

It is worth highlighting that the Sp-F1, A-F-S2, A-F-A1 and A-F-A2 points (Figure 6), which have not been used for regression purposes, seem not to belong to the curve obtained exploiting the fitting procedure. These points represent the only scenarios in which the analytical and Analytical-Lagrangian predictions satisfactorily reconstruct experimental observations, as it is reported in Table 13, where δ/t_{Jones} represents the deflection-thickness ratio lower and upper bound predictions from the Jones' theory, δ/t_N the empirical estimate using equation (6), δ/t_{AL} the deflection-thickness ratio registered in the Analytical-Lagrangian analyses and δ/t_{Exp} the respective experimental observation. No additional information is given about the A-F-S1 scenario, which, as already stated above, represents a close-range configuration not satisfactorily assessable by the methods used to build the database.

Scenario	δ/t_{Jones}	δ/t_N	δ/t_{AL}	δ/t_{Exp}
Sp-F1	[10.8, 15.2]	7.2	7.1	7.3
A-F-S2	[15.6, 19.8]	20.9	23.8	21.9
A-F-A1	[46.1, 58.8]	45.4	49.1	50.0
A-F-A2	[31.7, 40.6]	31.5	34.9	33.8

Table 13. Comparison of the δ/t results for the scenarios Sp-F1, A-F-S2, A-F-A1 and A-F-A2.

With regards to scenario B-H1, the analytical methods are not able to accurately describe the deflection-thickness ratio observed experimentally. A possible reason why that happens may be that the specific charge layout exploited in the campaign determined a planar blast wave impacting the structure, while the impulse prediction method adopted herein is valid for spherical or hemispherical detonations only [43]. However, the reflected impulse value, which was measured experimentally [5], may be exploited to determine the accurate dimensionless number ϕ which may be used to correctly classify the δ/t value. Such a procedure allows increasing the dimensionless number from 231 to 369, which further allows making accurate predictions compared to the experimental observations, as shown in Table 14.

Theory	δ/t prediction
Jones's Lower bound	208
Jones's Upper bound	262
Nurick and Martin	186
Equation (15)	185
Equation (16)	856
Experimental observation	187

Table 14. Updated results from scenario B-H1.

It is worth discussing the predictions shown above. The most accurate estimated values are the prediction by the Nurick and Martin's theory and that obtained from the equation (15) proposed in this work. Moreover, the prediction range from the Jones's analytical method seems to slightly overestimate the deflection-thickness ratio, while the prediction from equation (16) is, instead, wrong. This inaccurate prediction suggests that the quadratic formula obtained via model fitting to the numerical results only provides an accurate estimate when the dimensionless number is within the range of the ones characterising the numerical points from which the equation has been obtained.

To conclude, three hydrocode simulations are performed in ANSYS® AUTODYN® and are compared to the analytical results and to the experimental observations, if any. The selected scenarios are identified in Table 10 with the codes Sa-F1, Sa-F2 and V-F4. In these analyses, only mild steel plates are considered. The deflection-thickness ratio values are compared in Figure 7 for the selected scenarios.

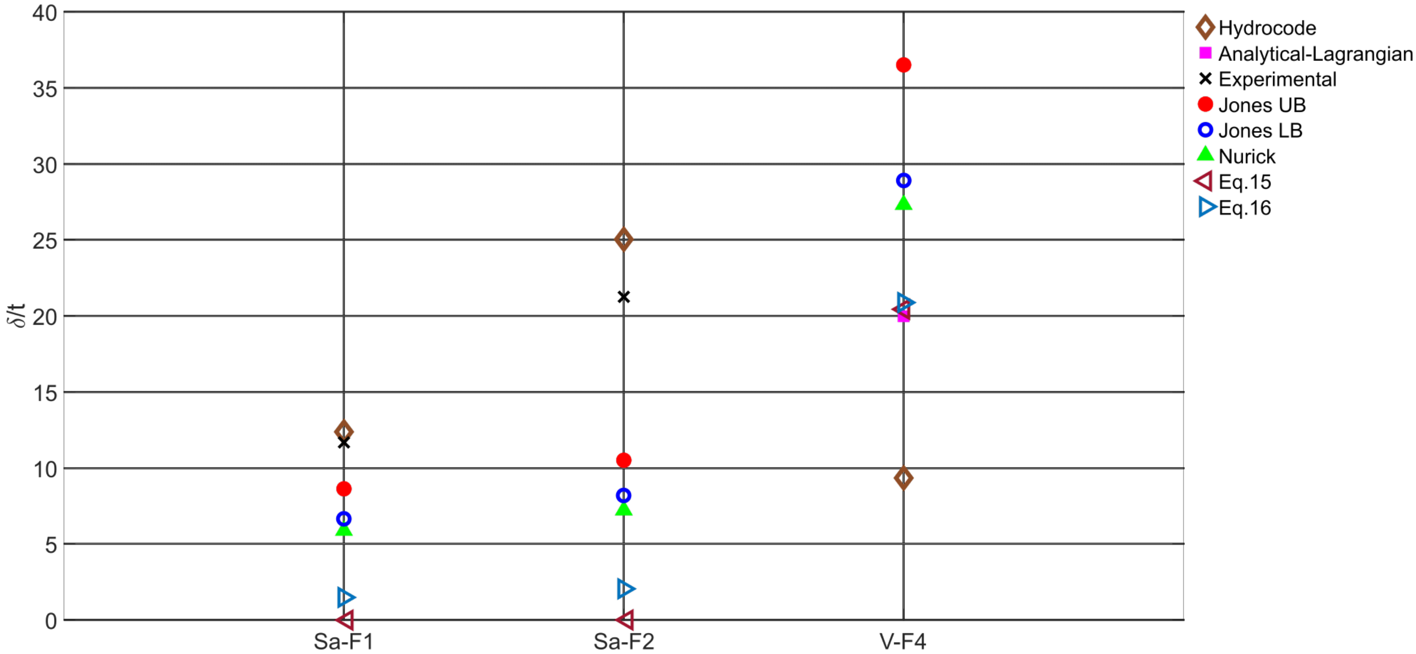

Figure 7. Results comparison considering hydrocode simulations.

The hydrocode simulations provide the most accurate predictions of the two analyses identified with the codes Sa-F1 and Sa-F2. It is interesting to note that these scenarios are identified in the subset SUB3, which cannot be assessed employing Analytical-Lagrangian simulations and analytical methods, as they tend to underestimate the predicted deflection-thickness ratio. Hence, the scenarios included in the subset SUB3 may be assessed by means of hydrocode analyses, which seem to successfully characterise blast waves in close-range configurations. However, to model more complex close-range phenomena such as afterburning, refined hydrocode analyses should be set up, which is out of the scope of this work. With regard to the free-field explosion V-F4, the empirical method of Nurick and Martin and the Jones' theory provide greater predicted permanent deflections than the estimates from the Analytical-Lagrangian analysis and the ones obtained through equations (15) and (16). In this last scenario, the hydrocode analysis seems to predict a lower deflection value than the Lagrangian analysis.

5 Conclusions

A detailed comparison of the performance of some predictive methods exploited to estimate the mid-point permanent transverse displacement of flat quadrangular plates has been reported in this work. In particular, the estimated values from two fully analytical methods, i.e., the Jones' and the Nurick and Martin's methods, have been compared to experimental observations and to the predictions from Analytical-Lagrangian and hydrocode numerical analyses.

In an effort to identify the potentialities of the methods involved, three subsets have been identified within the experimental results. In particular, for the subset SUB1, entirely composed of hemispherical detonations involving carpet-like charge layouts, two predictive equations, i.e., equations (15) and (16), have been proposed in this work, based on the curve fitting to the numerical results in agreement with the experimental observations. The application of the equations to a detonation scenario not considered among the regression data (B-H1) has shown that equation (15) provides the most accurate observed-value prediction compared to the analytical and numerical results, while equation (16) seems not to be valid outside the range within which the regression data lay. Moreover, close-range scenarios have been demonstrated to need hydrocode analyses to be satisfactorily predicted, even though more complex and refined analyses than the simulations presented herein have to be set up to accurately represent the underlying physics. Instead, either the analytical theory from Jones or the empirical method from Nurick and Martin may be exploited to evaluate the scenarios within the subset SUB2. In particular, it has been identified that those scenarios characterised by (i) spherical charge layout and (ii) limited radial expansion of the shock front value at the plate location, i.e., $\bar{r}_{plate} \in [12.5, 27.7]$ for the scenarios considered in this work, are satisfactorily characterised by employing the analytical approaches and the Analytical-Lagrangian methodology compared in this work.

Furthermore, it has been highlighted that no agreement on the impulse to consider in the dimensionless number ϕ definition is currently present in the literature. In fact, some works use the incident impulse, while others consider the effective impulse imparted to the structure, as also done in this work.

Further work needs to be conducted to provide more accurate predictive equations and to clearly identify the properties of each subset identified in this work, allowing to define a priori the most accurate predictive method to be employed to assess a specific scenario. Moreover, experimental campaigns involving both free-field detonations and ballistic steel plates may be conducted to compare the observations with the Analytical-Lagrangian estimates.

6 Bibliography

[1] R. Teeling-Smith and G. Nurick, “The deformation and tearing of thin circular plates subjected to impulsive loads,” International Journal of Impact Engineering, vol. 11, pp. 77-91, 1991.

[2] T. Wierzbicki and G. Nurick, “Large deformation of thin plates under localised impulsive loading,” International Journal of Impact Engineering, vol. 18, pp. 899-918, 1996.

[3] S. Yao, D. Zhang and F. Lu, “Dimensionless numbers for dynamic response analysis of clamped square plates subjected to blast loading,” Archive of Applied Mechanics, vol. 85, pp. 735-744, 2015.

[4] S. Chung Kim Yuen and G. Nurick, “Experimental and numerical studies on the response of quadrangular stiffened plates. Part I: subjected to uniform blast load,” International Journal of Impact Engineering, Vols. 55-83, p. 31, 2005.

[5] T. Børvik, A. G. Hanssen, M. Langseth and L. Olovsson, “Response of structures to planar blast loads – A finite element engineering approach,” Computers and Structures, vol. 87, pp. 507-520, 2009.

[6] E. L. Lee, H. C. Hornig and J. W. Kury, “Adiabatic Expansion of High Explosive Detonation Products,” Lawrence Radiation Laboratory, Livermore, CA, 1968.

[7] G. Randers-Pehrson and K. A. Bannister, “Airblast Loading Model for DYNA2D and DYNA3D,” Army Research Laboratory, Aberdeen Proving Ground, MD, 1997.

[8] N. Jones, “A Theoretical Study of the Dynamic Plastic Behaviour of Beams and Plates with Finite-Deflections,” International Journal of Solids and Structures, vol. 7, pp. 1007-1029, 1971.

[9] N. Jones, R. N. Griffin and R. E. Van Duzer, “An experimental study into the dynamic plastic behavior of wide beams and rectangular plates,” International Journal of Mechanical Sciences, vol. 13, no. 8, pp. 721-735, 1971.

[10] N. Jones, T. O. Uran and S. A. Tekin, “The dynamic plastic behaviour of fully clamped rectangular plates,” International Journal of Solids and Structures, vol. 6, pp. 1499-1512, 1970.

[11] T. X. Yu and F. L. Chen, “The large deflection dynamic plastic response of rectangular plates,” International Journal of Impact Engineering, vol. 12, no. 4, pp. 605-616, 1992.

[12] S. Bodner and P. Symonds, “Experiments on Viscoplastic Response of Circular Plates to Impulsive Loading,” Journal of the Mechanics and Physics of Solids, vol. 27, pp. 91-113, 1979.

[13] N. Perrone and P. Bhadra, “A Simplified Method to Account for Plastic Rate Sensitivity With Large Deformations,” Journal of Applied Mechanics, vol. 46, pp. 811-816, 1979.

[14] N. Jones, Structural Impact, II ed., Cambridge University Press, 2012.

[15] N. Jones, “Dynamic inelastic response of strain rate sensitive ductile plates due to large impact, dynamic pressure and explosive loadings,” International Journal of Impact Engineering, vol. 74, pp. 3-15, 2014.

[16] W. Johnson, Impact Strength of Materials, London: Edward Arnold, 1972.

[17] G. N. Nurick and J. B. Martin, “Deformation of Thin Plates Subjected to Impulsive Loading - A Review - Part I: Theoretical Considerations,” International Journal of Impact Engineering, vol. 8, no. 2, pp. 159-170, 1989.

[18] G. N. Nurick and J. B. Martin, “Deformation of Thin Plates Subjected to Impulsive Loading - A Review - Part II: Experimental Studies,” International Journal of Impact Engineering, vol. 8, no. 2, pp. 171-186, 1989.

[19] H. Babaei and T. M. Mostofi, “New dimensionless numbers for deformation of circular mild steel plates with large strains as a result of localized and uniform impulsive loading,” Proc IMechE Part L: J Materials: Design and Applications, vol. 234, no. 2, pp. 231-245, 2020.

[20] B. C. Cerik, “Damage assessment of marine grade aluminium alloy-plated structures due to air blast and explosive loads,” Thin-Walled Structures, vol. 110, pp. 123-132, 2017.

[21] A. S. Fallah, K. Micallef, G. S. Langdon, W. C. Lee, P. T. Curtis and L. A. Louca, “Dynamic response of Dyneema®HB26 plates to localised blast loading,” International Journal of Impact Engineering, vol. 73, pp. 91-100, 2014.

[22] T. M. Mostofi, H. Babaei, M. Alitavoli, G. Lu and D. Ruan, “Large transverse deformation of double-layered rectangular plates subjected to gas mixture detonation load,” International Journal of Impact Engineering, vol. 125, pp. 93-106, 2019.

[23] B. Park and S. Cho, “Simple design formulae for predicting the residual damage of unstiffened and stiffened plates under explosion loadings,” International Journal of Impact Engineering, vol. 32, pp. 1721-1736, 2006.

[24] M. Rezasefat, T. M. Mostofi, H. Babaei, M. Ziya-Shamami and M. Alitavoli, “Dynamic plastic response of double-layered circular metallic plates due to localized impulsive loading,” Proc IMechE Part L: J Materials: Design and Applications, vol. 233, no. 7, pp. 1449-1471, 2019.

[25] S. Yao, D. Zhang and F. Lu, “Dimensionless number for dynamic response analysis of box-shaped structures under internal blast loading,” International Journal of Impact Engineering, vol. 98, pp. 13-18, 2016.

[26] M. Ziya-Shamami, H. Babaei, T. M. Mostofi and H. Khodarahmi, “Structural response of monolithic and multi-layered circular metallic plates under repeated uniformly distributed impulsive loading: An experimental study,” Thin-Walled Structures, vol. 157, 2020.

[27] S. Chung Kim Yuen, G. N. Nurick, G. S. Langdon and Y. Iyer, “Deformation of thin plates subjected to impulsive load: Part III - an update 25 years on,” International Journal of Impact Engineering, vol. 107, pp. 108-117, 2016.

[28] S. Chung Kim Yuen, G. N. Nurick, W. Verster, N. Jacob, A. R. Vara, V. H. Balden, D. Bwalya, R. A. Govender and M. Pittermann, “Deformation of mild steel plates subjected to large-scale explosions,” International Journal of Imapact Engineering, vol. 35, pp. 684-703, 2008.

[29] Z. Xu, Y. Liu and F. Huang, “Deformation and failure of thin plate structures under blast loading,” Advances in Mechanical Engineering, vol. 11, no. 1, pp. 1-10, 2019.

[30] G. Langdon, W. Lee and L. Louca, “The influence of material type in the response of plates to air-blast loading,” Internation Journal of Impact Engineering, vol. 78, pp. 150-160, 2015.

[31] K. Safari, J. Zamani, S. Khalili and S. Jalili, “Experimental, theoretical, and numerical studies on the response of square plates subjected to blast loading,” Journal of Strain Analysis, vol. 46, pp. 805-816, 2011.

[32] K. Spranghers, I. Vasilakos, D. Lecompte, H. Sol and J. Vantomme, “Numerical simulation and experimental validation of the dynamic response of aluminum plates under free air explosions,” International Journal of Impact Engineering, vol. 54, pp. 83-95, 2013.

[33] V. Aune, G. Valsamos, F. Casadei, M. Larcher, M. Langseth and T. Børvik, “Numerical study on the structural response of blast-loaded thin aluminium and steel plates,” International Journal of Impact Engineering, vol. 99, pp. 131-144, 2017.

[34] V. Aune, E. Fagerholt, K. O. Hauge, M. Langseth and T. Børvik, “Experimental study on the response of thin aluminium and steel plates subjected to airblast loading,” International Journal of Impact Engineering, vol. 90, pp. 106-121, 2016.

[35] T. Børvik, A. G. Hanssen, S. Dey, H. Langberg and M. Langseth, “On the ballistic and blast load response of a 20ft ISO container protected with aluminium panels filled with a local mass – Phase I: Design of protective system.,” Engineering Structures, vol. 30, no. 6, pp. 1605-1620, 2008.

[36] T. Børvik, A. Burbach, H. Langberg and M. Langseth, “On the ballistic and blast load response of a 20ft ISO container protected with aluminium panels filled with a local mass – Phase II: Validation of protective system.,” Engineering Structures, vol. 30, pp. 1621-1631, 2008.

[37] T. M. Mostofi, H. Babaei and M. Alitavoli, “Theoretical analysis on the effect of uniform and localized impulsive loading on the dynamic plastic behaviour of fully clamped thin quadrangular plates,” Thin-Walled Structures, vol. 109, pp. 367-376, 2016.

[38] D. Hyde, “Microcomputer Programs CONWEP and FUNPRO, Applications of TM 5-855-1, 'Fundamentals of Protective Design for Conventional Weapons',” U.S. Army Corps of Engineers Waterways Experiment Station Instruction, Vicksburg, MS, 1988.

[39] J. M. Dewey, “The Friedlander Equations,” in Blast Effects. Physical Properties of Shock Waves., I. Sochet, Ed., Springer International Publishing, 2018, pp. 37-55.

[40] A. Ullah, F. Ahmad, H. Jang and e. al., “Review of Analytical and Empirical Estimations for Incident Blast Pressure,” KSCE Journal of Civil Engineering, vol. 21, pp. 2211-2225, 2017.

[41] Department of Defense - United States of America, “UFC 3-340-02 - Structures to Resist the Effects of Accidental Explosions,” 2008.

[42] G. F. Kinney and K. J. Graham, Explosive Shocks in Air, II ed., Springer-Verlag Berlin Heidelberg, 1985.

[43] L. Lomazzi, M. Giglio and A. Manes, “Analysis of the blast wave – structure interface phenomenon in case of explosive events,” IOP CONF. SER. MATER. SCI. ENG, Accepted.

[44] C. N. Kingery and G. Bulmash, Airblast Parameters from TNT Spherical Air Burst and Hemispherical Surface Burst, Maryland: Defence Technical Information Center, Ballistic Research Laboratory, Aberdeen Proving Ground, 1984.

[45] B. Hopkinson, “British ordnance board minutes, Report 13565,” British Ordnance Office, London, 1915.

[46] K. J. Cranz, O. v. Eberhard and K. E. Becker, Lehrbuch der Ballistik. Ergänzungen zum. Band II, Berlin: Springer, 1926.

[47] T. Krauthammer, Modern Protective Structures, Boca Raton, FL: CRC Press, 2008.

[48] T. Børvik, S. Dey and A. Clausen, “Perforation resistance of five different high-strength steel plates subjected to small-arms projectiles,” International Journal of Impact Engineering, pp. 948-964, 2009.

[49] E. Voce, “The relationship between stress and strain for homogeneous deformation,” J Inst Met, pp. 536-562, 1948.

[50] G. R. Johnson and W. H. Cook, “A constitutive model and data for metals subjected to large strains, high strain rates and high temperatures,” in Proceedings of seventh international symposium on ballistics, The Hague, The Netherlands, 1983.

[51] M. A. Iqbal, K. Senthil, P. Bhargava and N. K. Gupta, “The characterization and ballistic evaluation of mild steel,” International Journal of Impact Engineering, vol. 78, pp. 98-113, 2015.

[52] O. Atoui, A. Maazoun, B. Belkassem, A. Jonet, L. Pyl and D. Lecompte, “Numerical Investigation of Aluminium Plates Subjected to Blast Loading Using Arbitrary Lagrangian Eulerian and Lagrangian Approaches,” in SILOS proceedings (13th Shock and Impact Loads on Structures 2019), Singapore, 2019.

[53] C. M. Kaurin and M. O. Varslot, “Blast loading on square steel plates; A comparative study of numerical methods,” NTNU- Norwegian University of Science and Technology, 2010.

[54] LSTC, “LSTC support,” [Online]. Available: http://ftp.lstc.com/anonymous/outgoing/support/FAQ/damping. [Accessed 21 02 2020].

[55] N. Birnbaum, N. Francis and B. Gerber, “Coupled techniques for the simulation of fluid-structure and impact problems,” Computer Assisted Mechanics and Engineering Sciences, vol. 6, no. 3-4, pp. 295-311, 1999.

[56] N. Jha and B. S. K. Kumar, “Air Blast Validation Using ANSYS/AUTODYN,” International Journal of Engineering Research & Technology (IJERT), vol. 3, no. 1, 2014.

[57] Century Dynamics Inc., AUTODYN-2D and 3D v6.1 user documentation, Horsham, United Kingdom, 2005.

[58] B. Lusk, W. Schonberg, J. Baird, R. Woodley and W. Noll, “Using Coupled Eulerian and Lagrangian Grids to Model Explosive Interactions with Buildings,” in Proceedings of the 25th Army Science Conference, Orlando, FL, 2006.

[59] S. Malcolm, Autodyn theory manual, R 3.0, USA: Century Dynamics, 1997.

[60] J. Shin, A. Whittaker, D. Cormie and W. Wilkinson, “Numerical modeling of close-in detonations of high explosives,” Engineering Structures, vol. 81, pp. 88-97, 2014.

[61] J. Shin, A. Whittaker and D. Cormie, “TNT Equivalency for Overpressure and Impulse for Detonations of Spherical Charges of High Explosives,” International Journal of Protective Structures, vol. 6, no. 3, pp. 567-579, 2015.

[62] S. Rigby, A. Tyas, S. Clarke, S. Fay, J. Reay, J. Warren, M. Gant and I. Elgy, “Observations from Preliminary Experiments on Spatial and Temporal Pressure Measurements from Near-Field Free Air Explosions,” International Journal of Protective Structures, vol. 6, no. 2, pp. 175-190, 2015.